Low-order representation of the wake dynamics of offshore floating wind turbines

C Édric Raibaudo, L. Perret

12th International Symposium on Turbulence and Shear Flow Phenomena (TSFP12)
Osaka, Japan, July 19–22, 2022

LOW-ORDER REPRESENTATION OF THE WAKE DYNAMICS OF OFFSHORE FLOATING WIND TURBINES

Cédric Raibaudo, Laurent Perret
LHEEA
Centrale Nantes
1 Rue de la Noë, 44300 Nantes, France
cedric.raibaudo@univ-orleans.fr

Introduction

For the recent years, fixed and floating offshore wind turbine have been of particular interest for both scientific and industrial communities. A full understanding of wind turbines' wakes is crucial to improve their aerodynamical performances when operating in wind farms (Bastine *et al.*, 2018). For offshore wind turbines embedded in wind farms, multiple dynamics and phenomena impact the wake characteristics, including the influence of the incoming atmospheric boundary layer, the wake dynamics itself and the effect of the wave-induced motions. In particular, the influence of the surge motion due to the structure movement of a floating wind turbine, and the consideration of a realistic turbulent boundary layer have recently been touched on (Fu *et al.*, 2019; Schliffke *et al.*, 2020). However, available synthetic turbulence model for generating inflow conditions for simulations codes for performance and loads estimation are currently unable to account for all these interactions. Therefore, being able to model the complex dynamics of the wind turbine wake flow interacting with the atmospheric boundary layer to provide unsteady aeroelastic computational codes with realistic inlet conditions is of crucial importance.

The objective of the present study is to show the potential and validity of a low-order representation of the flow obtained from synchronized hot-wire anemometry (HWA) and Particle Image Velocimetry (PIV) measurements performed in the wind tunnel to accurately represent the wake flow dynamics. To this aim, realistic flow conditions are generated within the wind tunnel, ensuring that the incoming boundary layer and the wind turbine modeled by a porous disk are properly scaled. In addition, the porous disk can also translate along the longitudinal direction to mimic realistic surge-motion of a floating wind turbine. The velocity fields are reconstructed at high temporal resolution using a dimensionality reduction and reconstruction approach based on both POD and multi-time delay Stochastic Estimation, allowing for a detailed characterization of the dynamics of both the incoming boundary layer and the wake flow developing downstream of the model.

Experimental set-up

The experimental set-up is presented in Fig. 1. Experiments were performed in the LHEEA atmospheric wind tunnel. The free-stream velocity is $U_\infty = 4.0$ m/s and the turbulent intensity about 0.5%. The incoming boundary layer thickness is $\delta = 0.6$ m and the resulting Reynolds number is $Re = U_\infty \delta/\nu \approx 150000$.

The wind turbine is modeled with a porous disk of diameter $D = 0.16$ m and with the disk center ("hub") at height $z_{hub} = 0.12$ m. The model represents the 2 MW offshore floating wind turbine designed in the FLOATGEN project and put off the coast of Le Croisic, France. A sinusoidal surge motion is imposed on the model using a linear actuator. The amplitude of motion is $\pm 0.0625\ D$ and the actuation frequency $f^+ = fD/U_\infty = [\,0.00,\ 0.08,\ 0.12,\ 0.15]$. The motion parameters are chosen to be representative of the dynamical behavior of the wave-induced motion of the floating wind turbine.

The disk wake was characterized with Stereoscopic PIV (PIV-2D3C) in a $y-z$ plane normal to the main flow direction at two streamwise positions $x/D = 4.6$ and 8.1 downstream of the wind turbine model. The sampling frequency for the PIV is $F_{PIV} = 14.1$ Hz and 14000 snapshots were acquired. Constant temperature anemometry (CTA) measurements were also performed simultaneously to the Stereo-PIV. Twelve HWA sensors are distributed spanwise, downstream the PIV measurement plane and at two heights ($0.47D$ and $1.25D$). The sampling frequency for the HWA is $F_{HWA} = 15$ kHz. Sensors were calibrated using a King's law by measuring the free-stream flow with the help of a Pitot tube. These HWA acquisitions were considered, in addition to the wake documentation with one-point statistics and spectral analysis, to perform the linear stochastic estimation of time-resolved velocity fields.

Mean wake for fixed and floating wind turbines

These measurements were used to document the mean wake properties. Fig. 2 shows the streamwise RMS velocity σ_u/U_∞ for the model without motion at two streamwise positions of the PIV set-up. With respect to the streamwise position, the wake increases in radius but decreases in turbulence intensity. For floating wind turbines, the wave-induced motion could impact on the wake dynamics. The effect of the surge motion on the mean statistics is shown in Fig. 3. Streamwise RMS velocity profiles at hub height are considered for two streamwise positions and different frequencies of surge motion. The wake is similar in RMS for fixed and moving models at $x/D = 4.6$, slight differences are however observed for $x/D = 8.1$. Surge motions could make the wake structures convecting downstream more consistent.

Reconstruction using multi-delays POD-LSE

Spatial velocity fields measured by PIV and synchronized time-resolved velocity measurements using HWA are com-

bined for the reconstruction of the full spatio-temporal dynamics using a multi-time-delay Proper Orthogonal Decomposition and Linear Stochastic Estimation (mtd-POD-LSE) approach (Durgesh & Naughton, 2010). Velocity fields are decomposed into temporal and spatial modes using the classical snapshots POD:

$$\mathbf{u}(\mathbf{x},t) \approx \sum_{i=0}^{N_m} a_i(t)\, \Phi_i(\mathbf{x}) \tag{1}$$

with N_m the number of modes selected for the truncature. Here, $N_m = 100$ modes are chosen, corresponding to about 80% of the cumulative eigenvalues energy. The objective is to determine the more suitable coefficients B_{ijk} to express the relation between the temporal modes a_i and the HWA sensors with time delays τ_k:

$$a_i(t) = \sum_{j=0}^{N_j} \sum_{k=0}^{N_k} B_{ijk}\, S_j(t-\tau_k) \tag{2}$$

with $N_j = 12$ the number of HWA sensors S_j and N_k the number of delays imposed on the sensors. Here, $N_k = 21$ delays are distributed between ± 1 s, following previous reconstruction parameters on similar experiments (Blackman & Perret, 2016). The coefficients B_{ijk} are determined through the resolution of a least-square minimization problem using cross-correlations:

$$B_{ijk} \;=\; \mathscr{C}^{-1}_{\{a_i,\, S_{jk}\}}\, \mathscr{C}_{\{S_{jk}\}} \tag{3}$$

with $\mathscr{C}_{\{a_i,\, S_{jk}\}}$ the cross-correlations between the temporal modes and the sensors with delays, and $\mathscr{C}_{\{S_{jk}\}}$ the correlations between the different sensors with different delays. Temporal modes $\widehat{a_i}$ are therefore estimated at higher temporal resolution using Eq. 2, then combined with the spatial modes using POD (Eq. 1) to reconstruct the velocities. Two flow configurations considered for reconstruction are presented here, as important cases for their implementation in aeroelastic simulations: the turbulent boundary layer alone and the fixed model wake immersed in the turbulent boundary layer at $x/D = 8.1$. The sampling frequency used for the reconstruction is $F_s = 7.05$ kHz, to meet the conditions required for these simulations.

A first comparison of the first reconstructed temporal modes $\widehat{a_i}/\sqrt{2\lambda_i}$, with λ_i the POD eigenvalue of mode i, is performed in Fig. 4. These reconstructed modes $\widehat{a_i}$ are compared to the original modes a_i: strong correlation is observed for both chosen configurations, suggesting the reconstruction is consistent. It can be observed the distribution is slightly more scattered for the reconstruction of the wake than for the turbulent boundary layer, implying more difficulties to capture the flow complexity of the wake.

Reconstructed RMS velocity profiles along z are shown in Fig. 5. The statistics of the reconstructed velocities are compared with those of the original velocities obtained by the POD projection (Eq. 1) with the same number of modes $N_m = 100$ used for the mtd-POD-LSE process. For the turbulent boundary layer (Fig. 5 (a-b)), the streamwise and wall-normal velocity components, respectively σ_u/U_∞ and σ_w/U_∞, are well reconstructed. Only the spanwise component σ_v/U_∞ is underestimated of about 30% in average over the profile, more importantly far from the wall. PSD are also performed on the reconstructed streamwise velocity and compared with PSDs performed on the original velocity with the same amount of modes and on a hot-wire sensor ($n^\circ 10$ at $y/D = 0$ and $z/D = 1.25$). Spectrum is consistent at low frequency with the PIV and follows well the dynamics behavior of hot-wire sensor. A loss of spectrum amplitude is also observed between the two, suggesting a loss of information at higher frequency with the process due to the POD truncature and the limited number of sensors. Same analysis can be done for the reconstruction of the model wake at $x/D = 8.1$ (Fig. 5 (c-d)). All reconstructed velocities components are consistent with the original velocities. However, the reconstructed velocities are underestimated between 10% for σ_u/U_∞ to 19% for σ_w/U_∞. Even if the stochastic estimation looses information similarly to the TBL, these differences could also be linked to the conditioning of the correlation matrix during the POD-LSE process and will be improved by using Tikhonov regularization when solving the LSE least-square minimization problem. PSD of the reconstructed velocities are also consistent with the spectral analysis on the PIV and HWA. Spectra have more amplitude at low frequency, with peaks at $f^+ = \mathscr{O}(10^{-1})$, and reconstructed velocity PSD also capture this behavior at lower frequency.

Conclusions

Considering realistic conditions of the incoming flows of wind turbines has been proven to be of crucial importance. In the present study, velocity fields have been obtained experimentally for the turbulent boundary layer and wakes of fixed and moving porous disk corresponding to realistic behaviors of offshore wind turbines. The velocity has been reconstructed at high temporal resolution using mtd-POD-LSE. Spatio-temporal dynamics of the wake flow has been shown to be well captured by this low-order representation of the turbulent flow. In the full paper, a detailed analysis of the reconstructed velocity fields will be presented as a function of the flow configuration, including higher-order statistics of the three velocity components as well as velocity spectra. Based on the overall good performances of the reduction-reconstruction method presented here, future efforts will focus on using these data with high resolution in both time and space as inflow conditions for aero-elastic simulations of wind turbine loads.

REFERENCES

Bastine, D., Vollmer, L., Wächter, M. & Peinke, J. 2018 Stochastic wake modelling based on POD analysis. *Energies* **11** (3), 1–29.

Blackman, K. & Perret, L. 2016 Non-linear interactions in a boundary layer developing over an array of cubes using stochastic estimation. *Physics of Fluids* **28** (9).

Durgesh, V. & Naughton, J. W. 2010 Multi-time-delay LSE-POD complementary approach applied to unsteady high-Reynolds-number near wake flow. *Experiments in Fluids* **49** (3), 571–583.

Foti, D., Yang, X., Shen, L. & Sotiropoulos, F. 2019 Effect of wind turbine nacelle on turbine wake dynamics in large wind farms. *Journal of Fluid Mechanics* **869**, 1–26.

Fu, S., Jin, Y., Zheng, Y. & Chamorro, L.P. 2019 Wake and power fluctuations of a model wind turbine subjected to pitch and roll oscillations. *Applied Energy* **253**, 113605.

Schliffke, B., Aubrun, S. & Conan, B. 2020 Wind Tunnel Study of a "floating" Wind Turbine's Wake in an Atmospheric Boundary Layer with Imposed Characteristic Surge Motion. *Journal of Physics: Conference Series* **1618** (6).

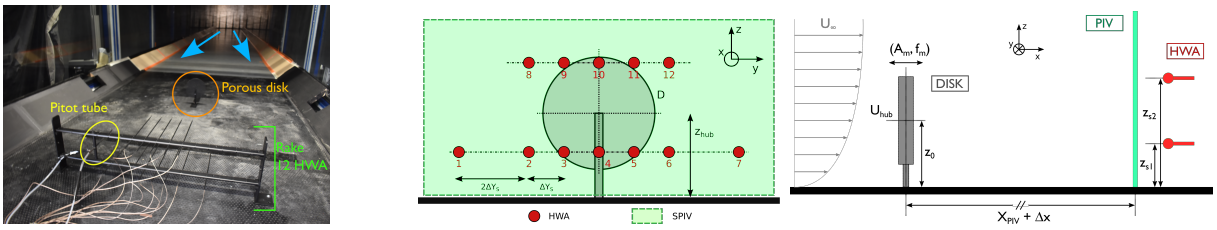

(a) (b)

Figure 1. Experimental set-up. (a) Set-up in the atmospheric wind-tunnel and (b) detailed scheme of the metrology used here.

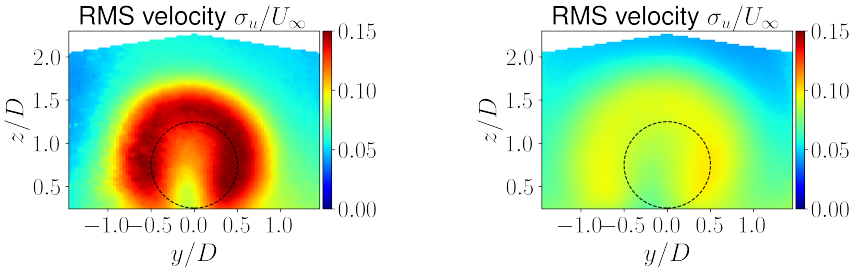

(a) (b)

Figure 2. Streamwise RMS velocity u/U_∞ for the fixed model wake at two PIV streamwise positions: (a) $x/D = 4.6$ and (b) $x/D = 8.1$. The dashed line circle shows the location of the wind turbine model at $x/D = 0$.

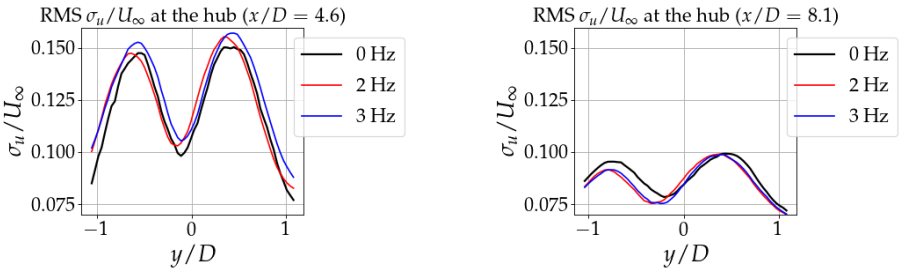

(a) (b)

Figure 3. RMS of the streamwise velocity component σ_u/U_∞ profile along y for the model wake for different surge motions at two PIV streamwise positions: (a) $x/D = 4.6$ and (b) $x/D = 8.1$.

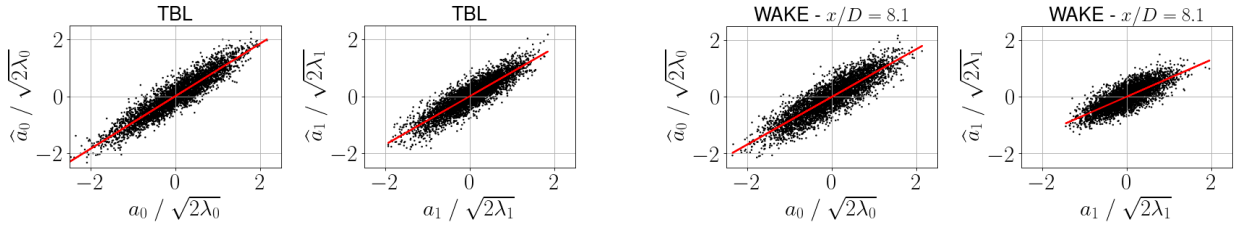

(a) (b) (c) (d)

Figure 4. Scatter plots for the first two reconstructed temporal mode $\widehat{a}_i/\sqrt{2\lambda_i}$ versus original mode $a_i/\sqrt{2\lambda_i}$ at two streamwise positions: (a-b) turbulent boundary layer without model, (c-d) $x/D = 8.1$.

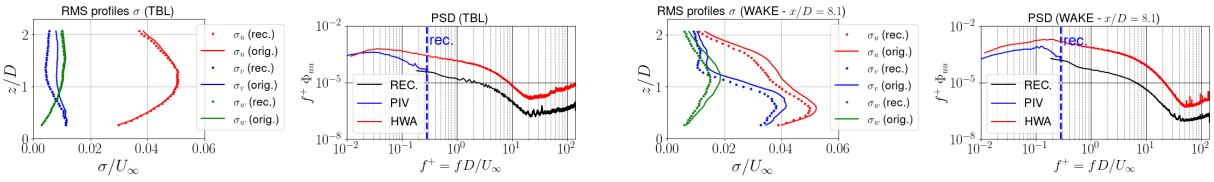

(a) (b) (c) (d)

Figure 5. (a,c) RMS of the reconstructed streamwise velocity component σ_u/U_∞ profiles along z using mtd-POD-LSE and original velocity using the same amount of modes $N_m = 100$ and (b,d) corresponding averaged pre-multiplied spectra. (a-b) turbulent boundary layer without model and (c-d) fixed model at $x/D = 8.1$.